Proceedings of the ASME 2022 Conference on Smart Materials, Adaptive Structures and Intelligent Systems
SMASIS2022
September 12-14, 2022, Dearborn, MI

SMASIS2022-92022

EFFECTS OF PENNATE ANGLE ON FAM BUNDLE HYDRAULIC EFFICIENCY FOR ROBOT ARM MOTION

Emily Duan
North Carolina State University
Raleigh, NC

Matthew Bryant
North Carolina State University
Raleigh, NC

ABSTRACT

This paper will investigate the effects of pennate angle on fluidic artificial muscle (FAM) bundles for a robot arm motion. Rising interest in soft fluidic actuators exists due to their prospective inherent compliance and safe human-robot interaction. The high force-to-weight ratio, innate flexibility, inexpensive construction, and muscle-like force-contraction behavior of McKibben FAMs make them an attractive type of soft fluidic actuator. Multi-unit architectures found in biological muscles tissues and geometric fiber arrangements have inspired the development of hierarchical actuators to enhance the total actuator performance and increase actuator functionality. Parallel, asymmetric unipennate, and symmetric bipennate are three muscle fiber arrangement types found in human skeletal muscle tissues. Unique characteristics of the pennate muscle tissue, with muscle fibers arranged obliquely from the line of muscle motion, enable passive regulation of effective transmission between the fibers and muscle. Prior studies developed an analytical model based on idealized assumptions to leverage this pennate topology in optimal fiber parameter design for FAM bundles under spatial bounds. The findings showed FAMs in the bipennate topology can be designed to amplify the muscle output force, contraction, and stiffness as compared to that of a parallel topology under equivalent spatial and operating constraints. This work seeks to extend upon previous studies by investigating the effects of pennate angle on actuation and system hydraulic efficiency for a robot arm with a more realistic FAM model. The results will progress toward tailoring actuator topology designs for custom compliant actuation applications.

Keywords: bioinspired, pennate muscle, soft actuators, McKibben muscle, muscle topology

1. INTRODUCTION

Conventional robot designs are composed of rigid joints and actuators to perform high-speed and force-demanding tasks. This equips rigid robots with large torque capacity and bandwidth. When provided sufficient sensing and advanced feedback control capability, rigid design robots' performance efficiency improves with full knowledge of their surroundings. Despite this, human behavior is unpredictable and cannot be programmed preemptively. Soft actuation solutions capture the importance of safety in human-robot interactions by the innate compliance of the materials used in the design. Of which, many are motivated by existing biological organisms. Unique attributes found in organic muscles have offered design inspiration to roboticists and researchers. The study of physiology and anatomy shows multiple motor units within biological muscle tissues. Hundreds to thousands of muscle fibers lie within a single motor unit and are arranged in a variety of topologies [1]. Hierarchical actuators leverage this multi-unit architecture to magnify actuators' performance and functionality [2]. Practical demonstrations of this hierarchical actuation strategy were used on cellular piezoelectric actuators [1], whiffletree actuators [2], series-parallel elastic actuators [3], and bioinspired orderly recruitment actuator bundles [4]. Linear actuator bundles improve efficiency through minimal consumed energy in the smallest required actuator unit [4,5]. Current studies have explored the parallel and pennate arrangement actuator bundle configurations. The parallel arrangement orients the longitudinal axis of individual actuators parallel to the bundle actuator line of motion. On the other hand, the pennate arrangement configures the longitudinal axis of individual actuators at an angle to the bundle actuator line of motion. While bundling heterogeneous pneumatic artificial muscles in a parallel arrangement allows for decoupling between stiffness and position [6], numerous biological studies have emphasized advantages in the pennate topology as well as identified the

effects of fiber pennation angle on the speed of contraction, damping of impact disturbances, and aging [7-12]. Pennate actuator studies show that a coupled relationship exists between fiber force and displacement to muscle force and displacement that allows for passive regulation of the effective gear ratio. A constitutive model developed for pennate actuators captures this behavior and has led to the characterization of pennate actuator bundles as variable stiffness actuators [10-13]. Moreover, effectively controlling variable stiffness aids in protecting humans in close proximity to robots by dampening effects from impact.

The muscle-like actuation behavior, inexpensive construction, inherent compliance, and high force-to-weight ratio of McKibben fluidic artificial muscles (FAMs) make them especially fitting for this application. Pennate McKibben bundle case studies have provided insight into how fibers (individual McKibben actuator units) should be arranged and what parameters should be varied for desirable force generation, contraction, and stiffness [11]. Although the sensitivity of FAM bundle actuation performance characteristics to pennation angle and fiber boundary conditions were established for spatial constraints, the implications of pennate FAM bundle actuation topology on hydraulic efficiency for a robot arm have yet to be explored.

This paper will investigate the effects of pennation angle on FAM bundle hydraulic efficiency for a specified robot arm motion. An idealized McKibben actuator model was used in collaboration with a model that accounts for FAM bladder elasticity to identify kinematic implications.

2. ROBOT ARM

A recommissioned robot arm from Cornell University designed for investigating variable recruitment strategies on fluidic artificial muscles (FAM) to simulate a human arm lifting weight was used as inspiration for this study [5]. Figure 1 displays the physical robot arm setup that is used to actuate a natural bicep curl motion. This setup was modeled in simulation to allow for quick tuning of various parameters highlighted in Table 1.

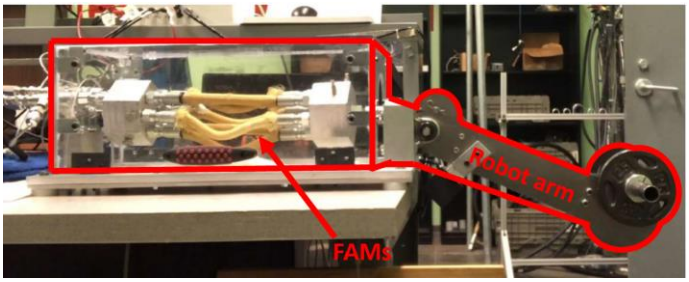

FIGURE 1: ROBOT ARM SETUP WITH HYDRAULIC FAMS

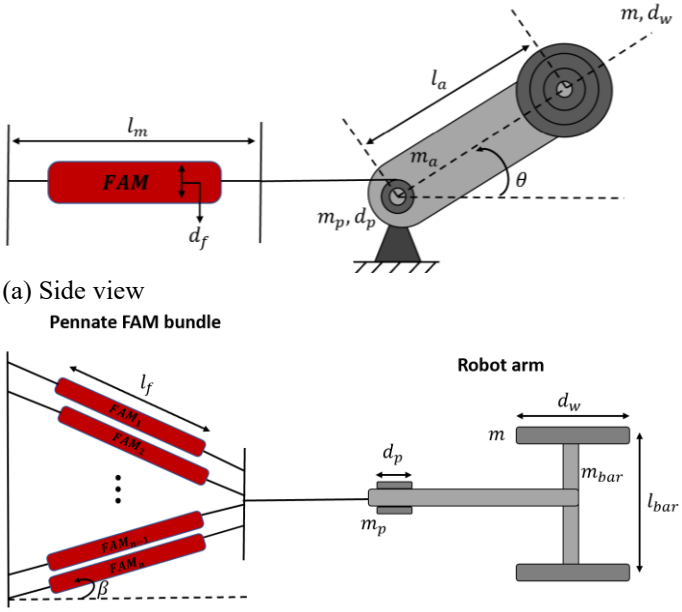

FIGURE 2: SCHEMATIC DIAGRAM OF SIMULATED ROBOT ARM SETUP

Simplified schematics of the robot arm are shown in Figure 2 to illustrate the side and top view of the robot arm setup. The FAMs are attached to a rigid structure connected to a pulley mechanism on the fixed position of the robot arm with weights loaded at the end of the arm.

Table 1: Robot arm parameters

Parameter	Variable	Value
Length of arm	l_a	$15.24\ cm\ (6\ in)$
Mass of arm	m_a	$0.028\ kg\ (0.0625\ lb)$
Mass of pulley	m_p	$0.028\ kg\ (0.0625\ lb)$
Diameter of pulley	d_p	$10.15\ cm\ (4\ in)$
Length of bar	l_{bar}	$10.15\ cm\ (1\ in)$
Mass of bar	m_{bar}	$0.028\ kg\ (0.0625\ lb)$
Diameter of weights	d_w	$5.08\ cm\ (1\ in)$
Mass of each end weight	m	$0.1134\ kg\ (0.25\ lbs)$

Robot arm parameters simulated in this study are described in Table 1. Muscle bundle displacement is characterized by $\Delta l_m = r_p\theta$, where θ is the desired robot arm rotation angle in radians. This study is focused on the effects of the initial pennation angle, β_i on the FAM bundle performance. Thus, the following FAM parameters described in Table 2 are held constant for this study.

Table 2: Fluidic artificial muscle parameters

Parameter	Variable	Value
Initial diameter of FAMs	d_{f0}	$1.905\ cm\ (0.75\ in)$
Initial length of FAMs	l_{f0}	$16.51\ cm\ (6.5\ in)$

Initial mesh braid angle	α_0	30°
Bladder thickness	t	1.59 mm (0.0625 in)
Number of FAMs	n	2

The FAMs are assumed to have pinned boundary conditions such that both ends of each FAM are fixed to a rigid structure connected to the pulley mechanism and the muscle bundle thickness is held constant during actuation. Thus, the muscle bundle displacement can also be expressed in terms of instantaneous FAM length l_f and pennation angle β as shown in (1).

$$\Delta l_m = r_p\theta = l_{f0}\cos(\beta_i) - l_f\cos(\beta) \tag{1}$$
$$\beta = \begin{cases} 0° \; if \; \beta_i = 0° \\ \sin^{-1}\left(\frac{\sin(\beta_i) l_{f0}}{l_f}\right) \; if \; 0° < \beta_i < 90° \\ 90° \; if \; \beta_i = 90° \end{cases}$$

3. METHODS

3.1 IDEAL MODEL VS. KLUTE-HANNAFORD MODEL

The ideal McKibben muscle is formulated by assuming the muscle behaves as a pressurized cylinder that shortens in length and expands radially subject to the internal pressure P on the mesh sleeve. Thus, the virtual work balance of the output force and internal pressure on the mesh shed light on the axial displacement and strain of the FAM. The predicted force of a single ideal McKibben muscle $F_{f,Ideal}$ is expressed in (2) with N number of turns the mesh fiber makes over the length of the FAM, $\lambda_1 = \frac{l_f}{l_{f0}}$, and B is the length of the mesh fiber [14].

$$F_{f,Ideal} = P\frac{3(\lambda_1 l_{f0})^2 - B^2}{4N^2\pi} \tag{2}$$
$$B = \frac{l_{f0}}{\cos(\alpha_0)} \qquad N = \frac{l_{f0}\tan(\alpha_0)}{2\pi r_{f0}}$$

However, characteristics such as bladder wall thickness, tapered geometry of the bladder, and friction between the bladder and mesh sleeve are not included in the ideal model. Experimental observations show notable variation with isobaric force-strain ideal model predictions [15]. An identified source of discrepancy stems from free strain dependence on pressure, which can be accounted for by incorporating bladder elastic forces opposing the mesh output force. Klute and Hannaford present an improved model that uses Mooney-Rivlin constants (C_{10}, C_{01}) to represent the nonlinear stress-strain relationship of the thin-walled bladder based on the bladder material [16]. Thus, the predicted force of a single FAM using the Klute-Hannaford model $F_{f,KH}$ shown in (3) is selected to understand the bladder elasticity effects on FAM performance. This study will assume the Mooney-Rivlin constants $C_{10} = 118.4\,kPa$ and $C_{01} = 105.7\,kPa$ for natural latex rubber. [16]

$$F_{f,KH} = F_{f,Ideal} + V_b\left\{\frac{1}{2l_{f0}^3\lambda_1^3}\left\{4(C_{10}+C_{01})\times l_{f0}^2(-1+\lambda_1^4) + \frac{4l_{f0}^6(-1+\lambda_1)\lambda_1^2(1+\lambda_1)(C_{10}+C_{01}\lambda_1^2)}{[-4N^2\pi^2r_{f0}^2+L_0^2(-1+\lambda_1^2)]^2} - \frac{4l_{f0}^4(C_{10}+C_{01}\lambda_1^4)}{-4N^2\pi^2r_{f0}^2+L_0^2(-1+\lambda_1^2)} - \frac{l_{f0}^4\lambda_1^4[C_{10}+C_{01}(-1+2\lambda_1^2)]}{N^2\pi^2r_{f0}^2}\right\}\right\} \tag{3}$$

The muscle bladder volume $V_b = n\pi l_{f0}t^2$ is constant assuming the bladder material is incompressible.

The model predicted force for a pennate FAM bundle can be rewritten as (4) and (5) to account for the number of FAMs in the bundle and the FAM pennation angle.

$$F_{m,Ideal} = nF_{f,Ideal}\cos(\beta) \tag{4}$$
$$F_{m,KH} = nF_{f,KH}\cos(\beta) \tag{5}$$

3.2 PENNATE FAM BUNDLE AND SYSTEM HYDRAULIC EFFICIENCY

To evaluate the effect of pennation angle on muscle bundle efficiency η_m and system hydraulic efficiency η_{hyd}, the desired robot arm actuation or work output must be held constant. Work output depends on the torque τ required to rotate the robot arm and the change in robot arm rotation angle $d\theta$. $\tau = I_{total}\ddot{\theta}$, where I_{total} is the total robot arm inertia and $\ddot{\theta} = \frac{d^2\theta}{dt^2}$ is the rotational acceleration. I_{total} is defined in (6) and damping is neglected.

$$I_{total} = I_{pulley} + I_{arm} + I_{bar} + 2I_{weight} \tag{6}$$
$$I_{pulley} = \frac{1}{2}m_p\left(\frac{d_p}{2}\right)^2$$
$$I_{arm} = \frac{1}{3}m_a l_a^2$$
$$I_{bar} = \frac{1}{12}m_{bar}l_{bar}^2 + m_{bar}l_a^2$$
$$I_{weight} = \frac{1}{2}m\left(\frac{d_w}{2}\right)^2 + m\left(\left(\frac{l_{bar}}{2}\right)^2 + l_a^2\right)$$

The difference in evaluating η_m as compared to η_{hyd} lies in the energy input, as expressed in the denominator of (7) and (8) respectively. The energy input depends on P for η_m and source pressure P_s for η_{hyd}. In addition, both energy inputs depend on the change in fluid muscle bundle volume dV_m. Thus, η_m allows for a fair comparison of pennate FAM bundle actuator performance.

$$\eta_m = \frac{\int \tau\, d\theta}{\int P dV_m} \tag{7}$$
$$\eta_{hyd} = \frac{\int \tau\, d\theta}{P_s \int dV_m} \tag{8}$$

Fluid muscle bundle volume is defined as $V_m = n\pi\left(\frac{d_f}{2}\right)^2 l_f$ for the ideal model and $V_m = n\pi\left(\frac{d_{f,inner}}{2}\right)^2 l_f$ for the Klute-

Hannaford model, where the d_f is the instantaneous FAM diameter and instantaneous inner FAM diameter $d_{f,inner} = d_f - 2t$. P_s is held constant at $517.11\ kPa$ $(75\ psi)$.

Given the explicit relationship between the desired robot arm rotation angle and corresponding instantaneous FAM length in (1) as well as the predicted muscle bundle output force with the ideal model in (2) and Klute-Hannaford model in (3), the instantaneous fluid muscle bundle volume and applied pressure can be evaluated to assess pennate FAM bundle efficiency and system hydraulic efficiency. Based on the desired robot arm actuation, only a range of β_i FAM bundle topologies are equipped with sufficient bundle stroke or displacement. A feasible range of β_i can be computed by solving for free bundle displacement $\Delta l_{m,free}$ for idealized McKibben actuators with (1), where $\beta_{free} = \sin^{-1}(\frac{\sin(\beta_i)\cos(\alpha_0)}{\cos(\tan^{-1}(\sqrt{2}))})$, $l_{f,free} = (\frac{\cos(\alpha_{free})}{\cos(\alpha_0)})l_{f0}$, and $\alpha_{free} = \cos^{-1}(\frac{\sin(\beta_i)\cos(\alpha_0)}{\sin(\beta_{free})})$. Furthermore, η_m=1 for idealized bipennate FAM bundles within this feasible range of β_i. This range of β_i is different from the Klute-Hannaford model due to pressure-dependent bundle free displacement. Such analysis is adequate for evaluating pennate FAM bundle efficiency. However, the viable range of β_i must further be refined with consideration of the source pressure for evaluating system hydraulic efficiency.

4. RESULTS

4.1 STROKE AND EFFICIENCY ANALYSIS

For the desired robot arm to rotate from a horizontal position or $\theta = 0°$ to $30°$ in 3 seconds, β_i of the feasible pennate muscle, bundle topologies range from $0°$ to $80.73°$ with the ideal model and $0°$ to $58.98°$ with the Klute-Hannaford model. To highlight the significance of considering FAM stroke dependence on pressure for pennate FAM bundles, Figure 3 compares the free bundle stroke between the ideal model and the Klute-Hannaford model to the initial pennation angle of the FAMs in the bundle at $P = 344.74\ kPa$ $(50 psi)$.

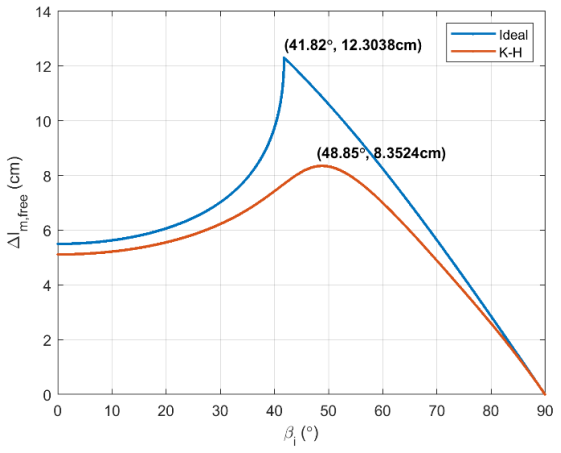

FIGURE 3: FREE PENNATE FAM BUNDLE STROKE

A simple oblique orientation of the FAMs in the bundle can allow for notable augmentation in free bundle stroke as seen with the ideal model. This peak occurs when the FAMs can fully contract and rotate. Though stroke amplification remains present with the inclusion of bladder elasticity effects, the magnitude shown with the Klute-Hannaford model is significantly less than the ideal model predicted and varies with the applied pressure.

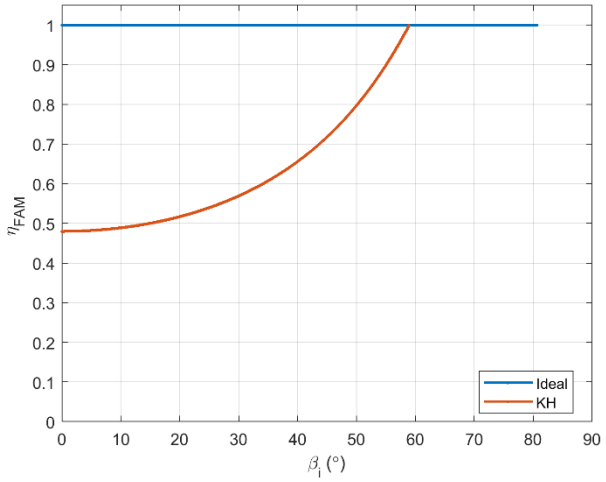

FIGURE 4: PENNATE MUSCLE BUNDLE EFFICIENCY

Figure 4 shows the pennate FAM bundle efficiency to the initial pennation angle for both the ideal model and the Klute-Hannaford model. The change in pennate FAM bundle fluid volume differs slightly with incorporating bladder elasticity from the Klute-Hannaford model. In addition, the wall thickness of the bladder drives up the pressure needed to reach the output force for the desired robot arm motion and $\eta_{FAM} < 1$.

For a source pressure of $13.79\ kPa$ $(2\ psi)$, the newly calculated β_i of feasible pennate muscle bundle topologies range is only slightly reduced from $80.73°$ to $78.81°$ for the ideal model and does not change for the Klute-Hannaford model. Figure 5 shows the system hydraulic efficiency to the initial pennation angle for both the ideal model and the Klute-Hannaford model.

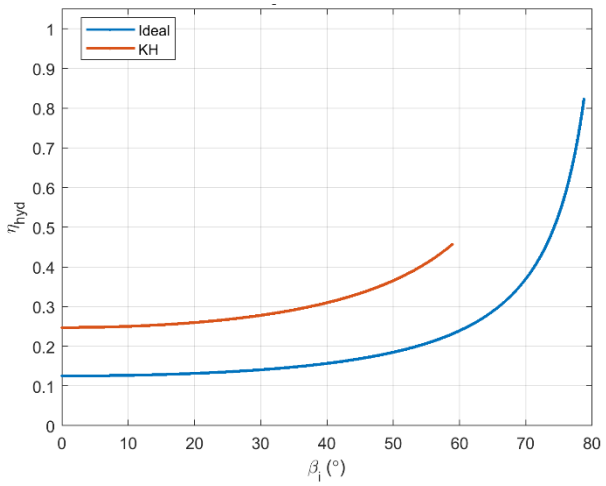

FIGURE 5: SYSTEM HYDRAULIC EFFICIENCY

Despite the predicted η_{FAM}, $\eta_{hyd} < \eta_{FAM}$ due to energy lost from throttling. Through analysis of system hydraulic efficiency with the ideal model, kinematic amplification can be isolated while the use of the Klute-Hannaford model facilitates the ability to detect bladder elasticity effects on pennate FAM bundle topology performance. It should be noted that the calculated hydraulic efficiency with the Klute-Hannaford model is greater than that of the ideal model. Figure 5 shows the most efficient pennate FAM bundle topology observed is just sufficient to achieve the desired robot arm task with no excess capacity for additional work and requires the least amount of pressure throttling.

4.2 SENSITIVITY ANALYSIS

Consequently, the pennation angle sensitivity to the desired robot arm actuation and operating conditions is of great interest. Robot arm inertia, desired rotation angle, and source pressure are individually examined to assess the performance of pennate FAM bundle topologies. Source pressure is explored first to observe not only the variation in pennate angle that maximizes hydraulic efficiency but also to evaluate the effects on hydraulic efficiency. For $12kPa < P_s < 137kPa$, the predicted initial pennation angle of the FAM bundle with maximum hydraulic efficiency and corresponding magnitude of hydraulic efficiency is shown in Figure 6 for both the ideal model and the Klute-Hannaford model.

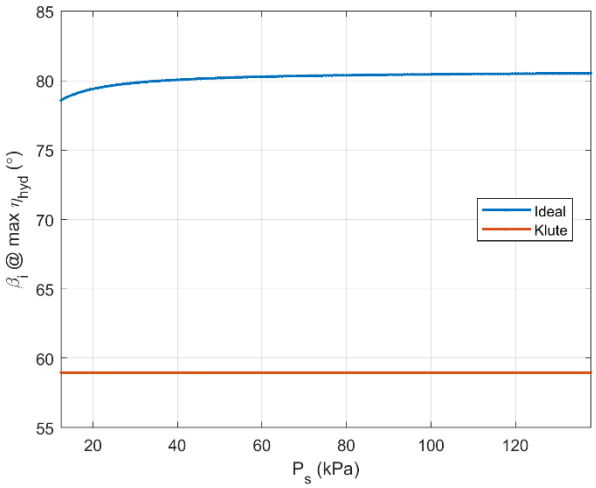

FIGURE 6: PENNATION ANGLE SENSITIVITY TO SOURCE PRESSURE

For both models, the initial pennation angle has little to no effect on source pressure. However, there is notable sensitivity to the hydraulic efficiency as shown in Figure 7.

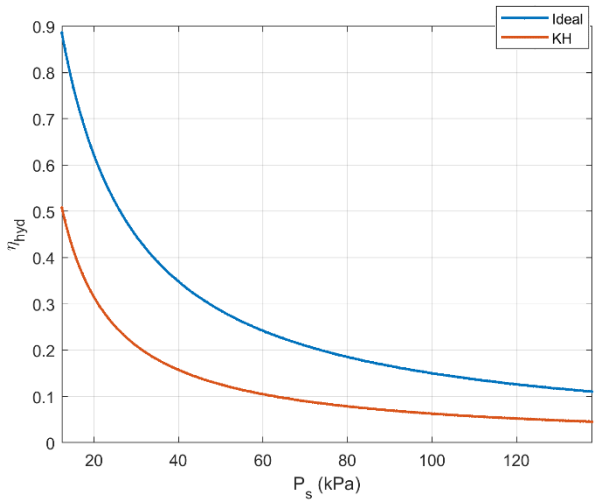

FIGURE 7: HYDRAULIC EFFICIENCY SENSITIVITY TO SOURCE PRESSURE

Choosing a source pressure that aligns with the operating pressure for the desired robot task prominently improves the hydraulic efficiency. Although a large source pressure can increase performance bandwidth, significant throttling is required to efficiently track the desired robot arm motion.

Next, a range of robot arm inertias is swept through by increasing the mass of end weights on the robot arm. Figure 8 shows the predicted initial pennation angle of the FAM bundle with maximum hydraulic efficiency as a function of robot arm inertia for both the ideal model and the Klute-Hannaford model. This analysis indicates the pennation angle of the maximum hydraulic efficiency is quite sensitive to the robot arm inertia.

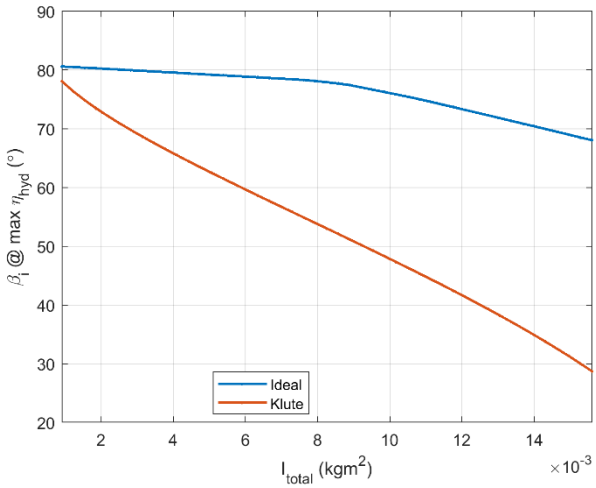

FIGURE 8: PENNATION ANGLE SENSITIVITY TO ROBOT ARM INERTIA

Figure 8 indicates the initial pennation angle with the maximum hydraulic efficiency decreases with increasing robot arm inertia. A larger robot arm inertia requires a greater output force from the bundle, which calls for a smaller initial pennation

angle. Furthermore, the calculated initial pennation angle with the Klute-Hannaford model that gives the maximum hydraulic efficiency remarkably decreases with robot arm inertia as compared to that with the ideal model. However, the hydraulic efficiency also varies with robot arm inertia as shown in Figure 9.

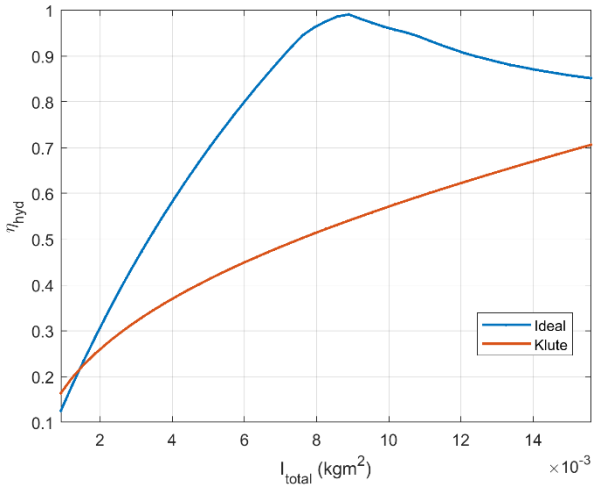

FIGURE 9: PENNATION ANGLE SENSITIVITY TO ROBOT ARM INERTIA

For the FAM parameters used in this study, hydraulic efficiency can be maximized for a specific robot arm inertia due to variation in bundle stroke. Thus, carefully sized pennate FAM bundle parameters can significantly improve hydraulic efficiency.

Across a span of robot arm rotation angles from 5° to 33°, the required muscle bundle displacement fluctuates as well as the corresponding output force to achieve the specified robot arm motion. Figure 10 plots the calculated initial pennation angles of the FAM bundle with maximum hydraulic efficiency from the ideal model and Klute-Hannaford model in correspondence with the robot arm rotation angle.

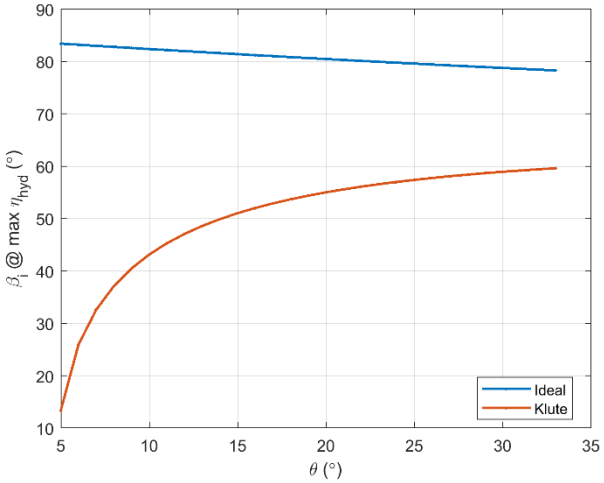

FIGURE 10: PENNATION ANGLE SENSITIVITY TO ROBOT ARM ROTATION ANGLE

The Klute-Hannaford model has pronounced pennation angle sensitivity to robot arm rotation angle as compared to the ideal model. The kinematic relationship observed for pennate FAM bundle actuation with the ideal model indicates a smaller initial pennation angle with maximum hydraulic efficiency should be expected for a large robot rotation angle. Conversely, an opposing trend is perceived with the Klute-Hannaford model, where bladder elasticity effects play a noteworthy role in bundle output force and fluid volume. Hence, the byproduct of this trend is increased hydraulic efficiency with a larger robot arm rotation angle.

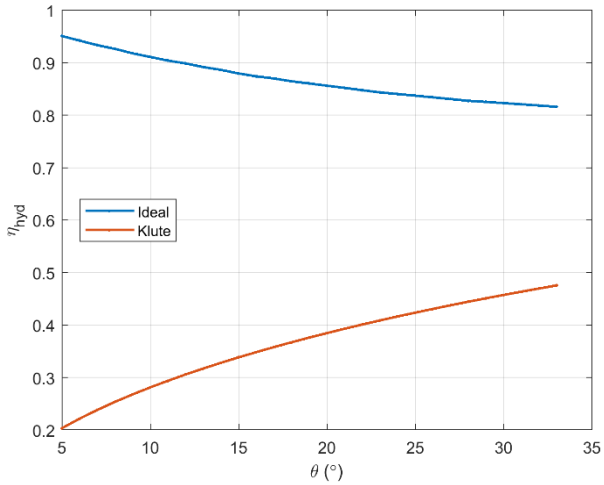

FIGURE 11: HYDRAULIC EFFICIENCY SENSITIVITY TO ROBOT ARM ROTATION ANGLE

5. CONCLUSIONS

This paper simulates the effect of pennation angle on fluidic artificial muscle bundle performance for robot arm motion. The use of the Klute-Hannaford model alongside the ideal model enables the ability to isolate the influence of bladder elasticity from kinematic amplification in pennate FAM bundle topologies. An analytical model that includes bladder elasticity effects improves the predicted behavior and performance of pennate FAM bundles. Pennate FAM bundle topologies just adequate to perform the desired robot arm actuation were observed to give the highest hydraulic efficiency. Robot arm inertia, rotation angle, and source pressure are separately examined for pennation angle sensitivity. The findings from this simulation provide insights on robot arm actuation and operating conditions for maximizing hydraulic efficiency. A pennate FAM bundle topology that calls for the least amount of throttling pressure is the most efficient to achieve the desired robot arm motion. In addition, hydraulic efficiency is maximum for the selected FAM bundle parameters at a specified robot arm inertia. Although pennate FAM bundle kinematics indicate a smaller initial pennation angle is needed for large robot arm rotation angles, bladder elasticity effects alter the bundle output force and fluid volume consumed to increase the hydraulic efficiency for bundles with large initial pennation angles.

Further work will explore the use of analytical models that include the effects of bladder wall thickness, braid elasticity as well as noncylindrical fluidic artificial muscle ends to extend our understanding of pennate FAM bundle performance. In addition, performance evaluation of pennation angle on spatially constrained FAM bundle topologies for a robot arm motion can provide insight into practical soft actuation designs. This investigation will enable progress toward the development of a framework for optimizing tissues to robot operating tasks and requirements.

ACKNOWLEDGEMENTS

The Faculty Early Career Development Program (CAREER) of the National Science Foundation under NSF Award Number 1845203 and Program Manager Irina Dolinskaya primarily supported this work.

REFERENCES

1. Ueda, J.; Schultz, A. Structure of cellular actuators. In *Cellular Actuators* **2017**, pp. 1-44
2. Huston, D.; Esser, B.; Spencer, G.; Burns, D.; Kahn, E. Hierarchical actuator systems. In Proceedings of the Society of Photo-Optical Instrumentation Engineers, San Diego, United States, 5 May 2005
3. Mathijssen, G.; Lefeber, D.; Vanderborght, B. Variable recruitment of parallel elastic elements: series-parallel elastic actuators (SPEA) with dephased mutated gears. *IEEE/ASME Transactions on Mechatronics* **2015**, *20*, 594-602
4. Bryant, M.; Meller, M.; Garcia, E. Variable recruitment fluidic artificial muscles: modeling and experiments. *Smart Materials and Structures*, **2014**, *23*
5. Meller, M.; Chipka, J.; Volkov, A.; Bryant, M.; Garcia, E. Improving actuation efficiency through variable recruitment hydraulic McKibben muscles: modeling, orderly recruitment control, and experiments. *Bioinspiration & Biomimetics* **2016** *11*
6. Giannaccini, M. et al Novel Design of a soft lightweight pneumatic continuum robot arm with decoupled variable stiffness and positioning, *Soft Robotics*, **2015**, *5*, 55-70
7. Robinson, R.; Kothera, C.; Wereley, N. Variable recruitment testing of pneumatic artificial muscles for Robotic Manipulators. *IEEE/ASME Transactions for Robotic Manipulators* **2015**, *20,* 1642-1652
8. Azizi, E.; Roberts, T. Variable gearing in a biologically inspired pneumatic actuator array. *Bioinspiration & Biomimetics* **2013**, *8*
9. Kianzad, S.; Pandit, M.; Lewis, J.; Berlingeri, A.; Haebler, KJ.; Madden, J. Variable stiffness structure using nylon actuators arranged in a pennate muscle configuration. In Proceedings of the Society of Photo-Optical Instrumentation Engineers, San Diego, United States, 29 April 2015
10. Betts, J. et al *Anatomy and Physiology* OpenStax, Rice University
11. Azizi, E.; Brainerd, E.; Roberts, T. Variable gearing in pennate muscles. *Proceedings of the National Academy of Sciences* **2008**, 105, 1745-1750
12. Jenkins, T.; Bryant, M. Pennate actuators: force, contraction, and stiffness. *Bioinspiration & Biomimetics.* **2020**, 15
13. Jenkins, T.; Bryant, M. Variable stiffness soft robotics using pennate muscle architecture. In Proceedings of the Society of Photo-Optical Instrumentation Engineers, Denver, United States, 13 March 2019
14. Tondu, B.; Lopez, P. Modeling, and control of McKibben artificial muscle robot actuators. *IEEE Control Systems*. **2000**, 20, 15-38
15. Duan, E.; Bryant, M. Implications of Spatially Constrained Bipennate Topology on Fluidic Artificial Muscle Bundle Actuation. *Actuators* **2022**, *11*, 82
16. Klute, G.; Hannaford, B. Accounting for Elastic Energy Storage in McKibben Artificial Muscle Actuators. ASME. *J. Dyn. Syst. Meas. Control*. **2000**, 122, 386–388